Precise determination of magnetic moment of a fluxoid quantum in a superconducting microring

Heonhwa Choi,[1,2] Yun Won Kim,[1] Soon-Gul Lee,[3] Mahn-Soo Choi,[4] Min-Seok Kim,[1] and Jae-Hyuk Choi[1,2,*]

[1]*Division of Physical Metrology, Korea Research Institute of Standards and Science, Daejeon 34113, Korea*
[2]*Department of Nanoscience, Korea University of Science and Technology, Daejeon 34113, Korea*
[3]*Department of Display and Semiconductor Physics, Korea University Sejong Campus, Sejong 30019, Korea*
[4]*Department of Physics, Korea University, Seoul 02841, Korea*

Using dynamic cantilever magnetometry and experimentally determining the cantilever's vibrational mode shape, we precisely measured the magnetic moment of a lithographically defined micron-sized superconducting Nb ring, a key element for the previously proposed subpiconewton force standard. The magnetic moments due to individual magnetic fluxoids and a diamagnetic response were independently determined at $T = 4.3$ K, with a subfemtoampere-square-meter resolution. The results show good agreement with the theoretical estimation yielded by the Brandt and Clem model within the spring constant determination accuracy.

I. INTRODUCTION

The superconducting ring has attracted considerable attention in the context of both fundamental superconductor research and application, because of its geometry-related effects, such as fluxoid quantization and quantum interference [1–5]. The magnetic flux, or more precisely, magnetic fluxoid, through an ordinary superconducting ring is quantized in units of $h/2e$, where h is Planck's constant and e is the electron charge [1]. In superconducting devices and applications, a superconducting ring with or without Josephson junctions has acted as a key element [4–8]. Understanding its magnetic properties is valuable for the design and analysis of, for example, a superconducting quantum interference device (SQUID) [4,5], a gravity gradiometry [6], an ultracold atom trap [7], and a subpiconewton force standard [8]. In particular, the concept of quantum-based force realization [8], which some authors have suggested as a candidate for the subpiconewton force standard previously, utilizes magnetic fluxoid quanta in a microscale superconducting ring. The force can be increased or decreased by a force step, estimated to be on the subpiconewton level, by controlling the fluxoid number. The magnetic moment due to a single fluxoid quantum is the minimum unit for generating a magnetic force in a well-defined magnetic field gradient.

Determining the unit magnetic moment with not only high sensitivity, but also high precision is key towards establishing the suggested method as the first standard for an extremely small force, because the unit magnetic moment defines the magnitude and precision of the unit force to be realized. Besides the small-force-standard application [8], the unit magnetic moment based on fluxoid quanta can be utilized as a new reference for a small magnetic moment at the femtoampere-square-meter level.

Several theoretical methods [9–11] have been developed to calculate the magnetic moments as well as the magnetic-field and current-density profiles for various values of the fluxoid number and external magnetic field in superconducting thin-film rings and disks. Initially, cases of negligibly small penetration depth λ were addressed [9,10], and Brandt and Clem [11] generalized the previous studies to finite λ, providing a calculation method to give precise numerical solutions. Although their theory has been adopted for superconducting ring design or to interpret its properties over the past decade [4,7,8], very few experimental studies providing high-precision measurements of the ring magnetic moment have been reported [2].

Experimentally, the measurement sensitivity for microsample magnetic moments is approaching its limit, as a result of the notable recent improvement in the force sensitivity in dynamic cantilever magnetometry [12–14] down to attonewton level [2,15]. In a study of persistent currents in normal metal rings [15], for example, dynamic cantilever magnetometry, which measures the resonance frequency shift of a cantilever in a magnetic field, exhibited a resolution that was approximately 250-fold superior to SQUID magnetometers [16,17] for detection of a ring's current. This result finally resolved previous order-of-magnitude discrepancies between experimental and theoretical current values. Such high sensitivity is obtained by applying high external fields. As regards dynamic cantilever magnetometry analysis of the low-field magnetic properties of a sample, however, a significant sensitivity reduction is inevitable. Very recently, this limitation was overcome using a phase-locked approach suggested by Jang *et al.* [2,18]. These researchers succeeded in detecting small half-fluxoid-quantum signals in an Sr_2RO_4 superconductor at low static fields by applying an additional oscillating field, which was phase locked to the cantilever position, for signal enhancement. The above studies have highlighted the potential sensitivity of dynamic cantilever magnetometry for magnetic-moment detection at both high and low magnetic fields.

In this work, we adopt dynamic cantilever magnetometry for precision measurement of the small magnetic moments of fluxoids in a superconducting microring. However, in order to retain a simple measurement geometry and to reduce the uncertainty factors, we do not employ a phase-locked approach, which requires precise control of the modulation field [18]. Instead, we enhance the resonance frequency shift by increasing the external field after trapping fluxoids in the ring. For a micron-sized Nb ring, we determine the magnetic moment of a single fluxoid, along with the Meissner susceptibility of the ring, and compare the results with

*jhchoi@kriss.re.kr

theoretical estimations from the Brandt and Clem method [11]. For accurate comparison, we prepare a ring sample with a well-defined geometry on an ultrasoft cantilever and utilize a fiber-optic interferometer with subnanometer resolution, with the fiber on a piezo positioner; this setup enables precision vibration measurement at multiple target positions on the cantilever. The latter is necessary for the experimental determination of the cantilever vibration mode characteristics, such as its effective length, which is otherwise theoretically estimated.

II. EXPERIMENT

For the sample-on-cantilever configuration, we batch-fabricate cantilevers with an Nb ring sample. After the cantilever patterns are defined in a low-pressure chemical vapor deposited (LPCVD) silicon-nitride layer on a silicon wafer, a 100-nm-thick Nb ring with nominal inner and outer radii of $a = 2$ and $b = 4$ μm, respectively, is fabricated via lift-off patterning with photolithography. The ring is aligned with the mounting paddle center of each cantilever, as can be seen in Fig. 1(b), (right). The cantilever fabrication is then completed, taking care to protect the attached, high-quality Nb film (see Ref. [19] for more details). The released cantilevers have 367 μm length, 4 μm width, and 200 nm thickness, with a mounting paddle at one end. The lateral dimensions and surface quality of the Nb ring are measured and examined using a Tescan Mira scanning electron microscope (SEM).

The sample-on-cantilever device is placed on a piezoactuator in high vacuum, surrounded by a superconducting solenoid for application of a uniform magnetic field. Its low-temperature vibration amplitude and resonance frequency are measured with a low-noise fiber-optic interferometer using a 1550-nm tunable laser (Agilent 81660B-200) with a high wavelength stability of 1 pm for 24 h and a coherence control feature, which has been demonstrated to have subpicometer resolution at an optical power of 10 μW and room temperature [20]. For our study, a very low laser power of 13 nW at the fiber end is adopted to avoid optical effects such as photothermal actuation. The fiber, attached to a three-axis piezo positioner, is located above a target position on the cantilever. The optical interference from the optical-fiber cantilever cavity is detected at a photodiode coupled to a low-noise transimpedance amplifier (Femtoamp DLPCA-200). The cantilever frequency

is primarily measured at a temperature of 4.3 K. In the magnetic-field-cooling (FC) process, the cantilever temperature is elevated momentarily using a light-emitting diode to above the superconducting transition temperature, T_c, of the Nb ring and then recovered. The entire system is mounted on a double-stage vibration-isolation platform including a 21-ton mass block.

Measurement fundamentals

Figure 1(a) shows the key features of our dynamic cantilever magnetometry setup. In an external magnetic field $\boldsymbol{H}_{\text{ext}}$, the magnetic moment $\boldsymbol{\mu}$ of the sample exerts a torque $\boldsymbol{\tau} = \boldsymbol{\mu} \times \boldsymbol{H}_{\text{ext}}$ on the cantilever. For a two-dimensional sample, we can assume that $\boldsymbol{\mu}$ has an out-of-plane component m only. Then, the magnitude of the torque is given as

$$\tau = m H_{\text{ext}} \sin \theta \tag{1}$$

and, with $\boldsymbol{H}_{\text{ext}} \parallel \boldsymbol{z}$, the relative angle θ of $\boldsymbol{\mu}$ and $\boldsymbol{H}_{\text{ext}}$ is identical to the cantilever surface angle at the sample position with respect to the $\boldsymbol{x}$ direction.

The shift of the resonance frequency f due to the magnetic torque [14,18] is expressed as

$$\Delta f = \frac{f_0}{2 k_0 L_{\text{eff}}^2} m H_{\text{ext}} = \frac{f_0}{2 k_0 L_{\text{eff}}^2} (\chi H_{\text{ext}} + n m_{\text{FQ}}) H_{\text{ext}}, \tag{2}$$

where k_0 and f_0 are the spring constant and intrinsic resonance frequency of the cantilever, respectively, and L_{eff} is the cantilever effective length. In the case of our superconducting ring, m has two contributions, from the diamagnetic response due to the Meissner current and from the n magnetic fluxoids in the ring hole. Here, χ is the Meissner susceptibility, and each fluxoid quantum has the same magnetic moment, m_{FQ}.

In our work, we adopt a cantilever, shown in Fig. 1(b), with $f_0 = 1221.9$ Hz and $k_0 = 4.5 \times 10^{-5}$ N/m in the fundamental vibrational mode. For L_{eff}, the theoretical value of $L/1.38$ for a rectangular Euler-Bernoulli beam of length L is frequently used [21]. However, the L_{eff} of our device was experimentally determined to be $L/1.48$ or 248 μm, by measuring the shape of the first vibration mode with a fiber on the piezo positioner. The minimum detectable frequency shift and magnetic moment, Δf_{min} and m_{min}, respectively, of our cantilever were estimated to be 1.1 mHz and 1.2 fAm^2, respectively, for a 1-Hz detection bandwidth with $H_{\text{ext}} = 40$ Oe. The characterization of the
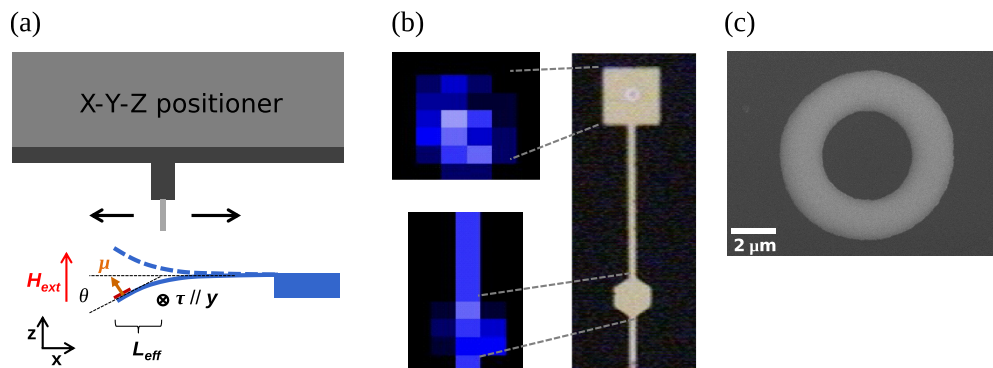

FIG. 1. (a) Schematic of dynamic cantilever magnetometry. (b) Optical microscope (right) and fiber scan (left) images of a free end part of a silicon nitride cantilever with a paddle (top) and a reflector (middle). (c) Calibrated SEM image of an Nb ring on a paddle (see Ref. [19]).
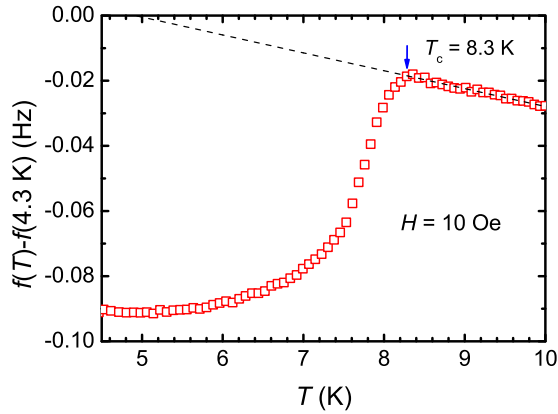
FIG. 2. Temperature dependence of the resonance frequency f of the Nb-ring-mounted cantilever in a magnetic field of 10 Oe, applied along the z direction after zero-field cooling. The arrow indicates the diamagnetic onset temperature of superconductivity. The dashed line is a linear fit to the data above $T = 8.4$ K.

cantilever mechanical properties is described in more detail in Appendix A.

III. RESULTS AND DISCUSSION

To observe the superconducting transition, the f of the cantilever was monitored with increasing temperature in a magnetic field of 10 Oe, applied perpendicularly to the mounted Nb ring after zero-field cooling to $T = 4.5$ K. The f temperature dependence exhibits a typical feature of a diamagnetic superconducting transition, with an onset temperature of $T_c = 8.3$ K, with the exception that a slope is apparent across the entire displayed temperature range (Fig. 2). This feature indicates that the superconducting ring is in the Meissner state at temperatures lower than T_c. The T_c value agrees well with the superconducting transition temperature obtained for a resistive measurement of a strip Nb sample from the same batch (data not shown here).

The f_0 in the absence of τ is represented by a dashed line in Fig. 2, having a slope of -5.5 mHz/K; this slope is obtained from a fit of the data in the normal state. The possible origins of the negative slope are the temperature dependence of the

cantilever dimensions, cantilever surface stress, and so on; further discussion of this topic is presented in Appendix B.

In the Meissner state of the Nb ring, the f response to sweeping H_{ext} follows Eq. (2), resulting in the parabolic curve shown in Fig. 3(a). The parabolic dependence is valid in the $|H_{ext}| \leqslant \sim 60$ Oe range, whereas it breaks down beyond this range as a result of magnetic vortex penetration into the annular area, i.e., a mixed state of Nb. Such a small critical field value is attributed to the high demagnetization effect due to the quasi-two-dimensional sample geometry [22]. As we increase the FC magnetic field, H_{FC}, used in cooling the Nb ring from above T_c, more magnetic fluxoids are contained within the ring hole. Accordingly, the curve is shifted to higher f and H_{ext}.

Parabolic fits to the data shown in Fig. 3(a) can provide χ and nm_{FQ}; however, we obtained the nm_{FQ} values from separate measurements, which proved to be more accurate and efficient. We deduced χH_{ext} by dividing the $H_{FC} = 0$ data by H_{ext}, which exhibits a linear dependence, as depicted in Fig. 3(b). Note that data at low magnetic fields were not employed, because of their low accuracy. The linear fit yields $\chi = -102 \pm 10$ pAm^2/T.

To observe individual magnetic fluxoids at $T = 4.3$ K, we varied H_{FC} from 10 to 13 Oe with a smaller step of 0.1 Oe. To enhance the Δf signal for nm_{FQ} for low H_{FC}, we increased the magnetic field from H_{FC} to a larger and fixed value, i.e., $H_{ext} = 40$ Oe, before measuring f. This procedure is depicted in the inset of Fig. 4. In this manner, we could obtain nm_{FQ} for small n, because nm_{FQ} is independent of the magnetic field, but its contribution to Δf is proportional to H_{ext}, as shown in Eq. (2). Note that the contributions of χH for various H_{FC} are identical and can be universally eliminated because H_{ext} is fixed. Figure 4 clearly shows that f has a stepwise feature with varying H_{FC}. The single step width, ΔH, was estimated to be 0.65 ± 0.03 Oe from the total width of the four steps fully shown in Fig. 4. Taking the errors in H_{FC} and ΔH into consideration, the n corresponding to $H_{FC} = 10$ Oe may range from 14 to 16.

For FC with a H_{FC} corresponding to the center of each step plateau, no net current circulates the ring, even with n fluxoids and the response to the external field. The effective area of the zero-current contour is given by $A_{eff} = \Phi_0/H_a$ [11], where H_a is the field increment necessary to induce a transition from the n to $n + 1$ state. Because $H_a = \Delta H$, we can estimate A_{eff} to be 32 μm^2, which indicates flux focusing where A_{eff} is larger
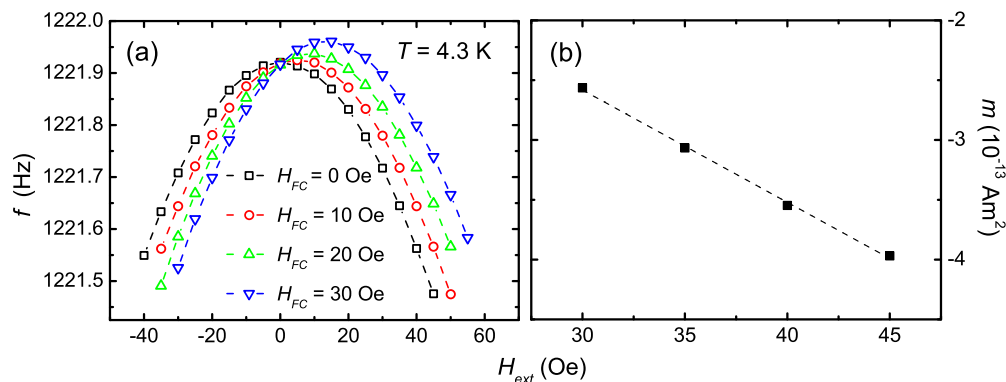

FIG. 3. (a) Resonance frequency f of the cantilever versus the external magnetic field, H_{ext}, for various values of H_{FC}, the magnetic field used in field cooling. (b) Diamagnetic response for increasing H_{ext}, calculated from the f shift for $H_{FC} = 0$ Oe. The dashed line is a linear fit.
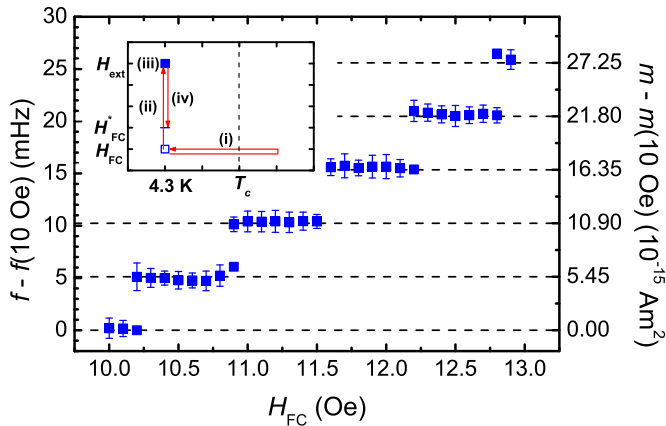
FIG. 4. Resonance frequency shift (left axis) and magnetic moment (right axis) vs H_{FC}. Each data point was obtained from five repetitions of a temperature-field cycle and a single measurement with an averaging time of 40 s, described in the inset: (i) warm-up and field cooling at H_{FC}; (ii) increasing field up to H_{ext}; (iii) f-shift measurement; and (iv) decreasing field to the next value, H_{FC}^*. The error bars indicate standard deviations, and the dashed lines are guides for the eye.

than the actual hole area, $\pi a^2 = 13\ \mu m^2$. This estimate agrees roughly with the $A_{eff} = 25\ \mu m^2$ result calculated using the Brandt and Clem theoretical prediction [11].

Within ΔH, f is virtually constant to within 1 mHz for changing H_{FC}, which implies that the number of fluxoids is fixed and their contribution to m is constant. As H_{FC} is raised beyond ΔH, an additional fluxoid is introduced to the ring hole, resulting in a discrete shift of f or m_{FQ} as shown in Fig. 4. As the m_{FQ} of each fluxoid are intrinsically expected to be equivalent, this value can be determined from the average

of the five steps of m or f, which are 5.8 ± 0.6 fAm^2 or 5.2 ± 0.2 mHz, respectively. Note that the uncertainty in the cantilever spring constant makes a dominant contribution to the estimated error in m_{FQ}. Near the step edges, f is observed at both fluxoid quantum numbers, n and $n + 1$, because the kinetic energies of the right- and left-circulating supercurrent states, respectively, are degenerate for Nb-ring cooling at corresponding magnetic fields.

Figure 5 depicts the theoretical values of the magnetic moments due to a single fluxoid and a diamagnetic response, which were estimated numerically for various ring radii utilizing the Brandt and Clem model [8,11]. As shown in the figure, the magnitudes of m_{FQ} and χ decrease slowly with increasing a, but increase with higher dependence with increasing b. The experimentally obtained values are also plotted at the dimensions of our Nb ring on the cantilever; the dimensions are measured from the calibrated SEM, yielding a and b of $2.0 \pm 0.1\ \mu m$ and $3.8 \pm 0.1\ \mu m$, respectively. For $\Lambda = 110$ nm at 4 K [23], where $\Lambda = \lambda^2/d$ is the thin-film penetration depth and d is the film thickness, m_{FQ} and χ are calculated to be 5.98 ± 0.10 fAm^2 and -91.2 ± 0.3 pAm^2/T (5.98 ± 0.24 fAm^2 and -91.2 ± 7.8 pAm^2/T), respectively, if the uncertainty of a (b) is considered. These values are in quite good agreement with the experimental results, considering the accuracy of the spring constant determination.

The effect of the Λ uncertainty is negligible, as m_{FQ} and χ are estimated to vary by only 1.4% and -1.7%, respectively, for a Λ difference of 10%. However, it is notable that the assumption of negligible Λ in the theoretical estimation yields $m_{FQ} = 7.17$ fAm^2 and $\chi = -116$ pAm^2/T, which are considerable overestimations in comparison with the experimental values. This finding implies that consideration of the finite penetration depth, as in the Brandt and Clem model, is crucial for appropriate description of micron-sized
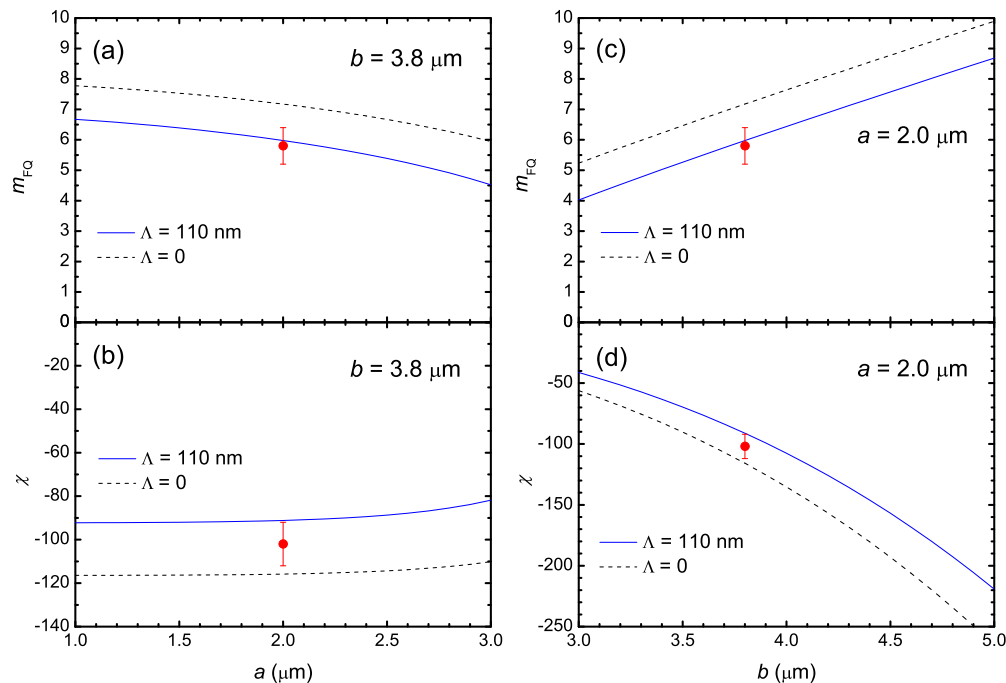

FIG. 5. Theoretical estimates of m_{FQ} and χ for $\Lambda = 0$ and 110 nm for a superconducting ring with varying inner radius a [(a) and (b)] and outer radius b [(c) and (d)]. The circles represent the experimental values with error bars indicating 10% accuracy.

superconducting rings, and that it remains valid when the ring radii uncertainty is considered, as can be seen in Fig. 5.

IV. CONCLUSIONS

Using high-resolution cantilever magnetometry capable of fiber scanning, we precisely measured the magnetic moment of a well-defined superconducting Nb thin-film ring with inner and outer radii of 2.0 and 3.8 μm, respectively, on an ultrasoft cantilever at $T = 4.3$ K. The experimental results, a diamagnetic response of -102 pAm^2/T and a single fluxoid magnetic moment of 5.8 fAm^2, agree well with the theoretical model prediction, providing a reliable technical and theoretical base for superconducting microring research and applications in the future.

APPENDIX: A

In dynamic cantilever magnetometry, the resonance-frequency shift Δf can be derived by calculating the magnetic torque oscillation dependent on the cantilever vibrations. The cantilever vibration is a solution of the equation of motion for beam vibration [24], which is generally expressed as

$$u(x,t) = \sum_{n=1}^{\infty} u_n(x)q_n(t), \qquad (A1)$$

where $u_n(x)$ is the nth resonance mode shape and $q_n(t)$ is the generalized coordinate in the nth mode. If we drive the cantilever at one of the resonance frequencies, for example, the first mode, the problem is reduced to solving a one-dimensional forced equation of motion for $q_1(t)$. The cantilever is subject to an effective force of τ/L_{eff}, where L_{eff} is the cantilever effective length, defined as $u_1(x)/\tan\theta = u_1(x)/[du_1(x)/dx]$ [21]. The effective force can then be deduced as

$$\frac{\tau}{L_{\text{eff}}} = \frac{1}{L_{\text{eff}}^2} m H_{\text{ext}} u_1(x) q_1(t) \qquad (A2)$$

from Eq. (1), with an approximation of $\sin\theta \cong \frac{du_1(x)}{dx} q_1(t) = \frac{u_1(x)}{L_{\text{eff}}} q_1(t)$ for small deflections. Hence, the Fourier transform of the forced vibration equation for $q_1(t)$ can be expressed as [18]

$$\left(-\omega^2 - i\gamma\omega + \omega_0^2\right)\tilde{q}(\omega) = \frac{\omega_0^2}{k_0 L_{\text{eff}}^2} m H_{\text{ext}} \tilde{q}(\omega). \qquad (A3)$$

Here, ω_0 is the angular resonance frequency $2\pi f_0$. The solution of Eq. (A3) gives Δf as expressed in Eq. (2) [14,18].

As illuminating the cantilever free end, even at small laser power, may cause local heating of the sample, Δf measurement for magnetometry is conducted with the fiber
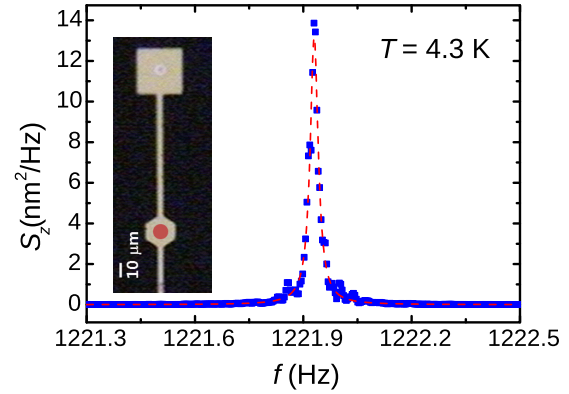

FIG. 6. Thermal vibration noise spectrum at $T = 4.3$ K measured at the reflector position (closed circle in the inset).

pointing at the center of a 20-μm-width reflector, shown in Fig. 1(b), 100 μm from the paddle on which an Nb ring is mounted. To align the fiber to the reflector center or another point of interest, we first obtain a quick map of the cantilever, as shown in Fig. 1(b), by scanning the cantilever plane and obtaining the laser interference amplitude at each point; this is achieved by sweeping the fiber-cantilever interdistance. Then, for fine adjustment, we repeatedly obtain line profiles of the interference amplitude, in directions both parallel and perpendicular to the cantilever, to find the target position with ~ 1 μm resolution.

To determine precise values for k_0 and L_{eff} in Eq. (2), we require a fundamental mode shape; therefore, we obtain position-dependent vibrational noise spectra along the cantilever. These spectra provide $\langle u^2(x,t) \rangle$ from Eq. (A1), which falls on the mode shape predicted by the finite element method for the cantilever employed in this work. From the ratio of $\langle u^2(x,t) \rangle$ at the sample position, $\langle u_S^2 \rangle$, against that at the reflector center, $\langle u_R^2 \rangle$, we determine the spring constant conversion factor, $\langle u_S^2 \rangle/\langle u_R^2 \rangle$, to be 2.85, and from the slope at the sample position, we determine L_{eff} to be 248 μm.

Figure 6 shows the fundamental thermal vibration noise spectrum at $T = 4.3$ K, obtained with a span of 3.125 Hz and averaging over 15 results, which provides $\langle u_R^2 \rangle$ as well as $f_0 = 1221.9$ Hz and the quality factor $Q = 43\,000$. Using the equipartition theorem along with $\langle u_S^2 \rangle/\langle u_R^2 \rangle$, the mechanical impedance to the force at the sample position is evaluated to be $k_0 = 4.5 \times 10^{-5}$ N/m, with an accuracy conservatively claimed to be 10% [25]. The minimum detectable shift of the cantilever frequency is given by $\Delta f_{\text{min}} = f_0 F_{\text{min}}/\sqrt{2}k_0 x_{\text{pk}}$ [14]. Here, F_{min} is the smallest detectable force signal, given by $F_{\text{min}} = \sqrt{2k_0 k_B T B/\pi f_0 Q}$, where k_B is the Boltzmann constant, x_{pk} is the peak displacement of the oscillating cantilever, and B is the detection bandwidth. The thermally limited detectable magnetic moment m_{min} can be expressed as $2\Delta f_{\text{min}} k_0 L_{\text{eff}}^2/f_0 H_{\text{ext}}$, employing Eq. (2). Using the cantilever parameters given above, the corresponding Δf_{min} and m_{min} are 1.1 mHz and 1.2 fAm^2 for a 1-Hz bandwidth with $x_{\text{pk}} = 100$ nm and $H_{\text{ext}} = 40$ Oe.

APPENDIX: B

The negative slope of $f_0(T)$ in Fig. 2 may originate from the temperature dependence of the Young's modulus, dimensions,

surface stress, and so on, of the silicon nitride cantilever. The spring constant of a simple beam is given by [21] $k_0 = 1.030 E w t^3 / l^3$, where E is the Young's modulus of the material and w, t, and l are the beam width, thickness, and length, respectively. With $2\pi f_0 = \sqrt{k_0/m_{\text{eff}}}$, where m_{eff} is the beam effective mass, the temperature derivative of $f_0(T)$ can be expressed as

$$\frac{1}{f_0}\frac{df_0}{dT} = \frac{1}{2k_0}\frac{dk_0}{dT} = \frac{1}{2}\left(\frac{1}{E}\frac{dE}{dT} + \frac{1}{w}\frac{dw}{dT}\right), \quad \text{(B1)}$$

where we assume an isotropic thermal contraction for w, t, and l.

The effect of the intrinsic Young's modulus can be ignored because, in general, its temperature dependence is virtually zero at low temperatures. If we adopt the Wachtman semiempirical formula for Young's modulus [26], $E(T) = E_0 - BT \exp(-T_0/T)$, its temperature derivative is given by $dE/dT = -B(1 + T_0/T)\exp(-T_0/T)$. For the reported parameters for silicon nitride [26], $E_0 = 320$ GPa, $B = 0.0151$ GPa/K, and $T_0 = 445$ K, $(1/E)dE/dT$ is estimated to be as small as -1×10^{-24} K^{-1} at $T = 9$ K.

Excluding the intrinsic Young's modulus, we may speculate that the temperature dependence of the cantilever dimensions yields the $f_0(T)$ slope both indirectly and directly, via the first and second terms on the right-hand side of Eq. (B1), respectively. One possible indirect effect is via surface stress in a thin cantilever. Because of the strain-dependent surface stress, the effective Young's modulus E_{eff} of a silicon nitride cantilever has been reported to have a thickness dependence [27]. That is, E_{eff} decreases strongly for decreasing thickness below our cantilever thickness of 200 nm.

Considering the thickness dependence and the signs in Eq. (B1), the thermal contraction of the cantilever dimensions for increasing T is consistent with the negative slope of $f_0(T)$, if other factors are ignored. The lower bound of the thermal expansion coefficient α, which is defined as $\alpha = (1/w)dw/dT$, can be estimated from Eq. (B1) with the assumption of $dE/dT = 0$, yielding $\alpha_{\text{lower}} = (2/f_0)df_0/dT = -9 \times 10^{-6}$ K^{-1}. More systematic studies are necessary in the future to determine an accurate value of α for silicon nitride at low temperatures.

[1] M. Tinkham, *Introduction to Superconductivity*, 2nd ed. (McGraw-Hill, New York, 1996).

[2] J. Jang, D. G. Ferguson, V. Vakaryuk, R. Budakian, S. B. Chung, P. M. Goldbart, and Y. Maeno, Science **331**, 186 (2011).

[3] C.-T. Chen, C. C. Tsuei, M. B. Ketchen, Z.-A. Ren, and Z. X. Zhao, Nat. Phys. **6**, 260 (2010).

[4] K. Hasselbach, C. Ladam, V. O. Dolocan, D. Hykel, T. Crozes, K. Schuster, and D. Mailly, J. Phys.: Conf. Ser. **97**, 012330 (2008).

[5] J. R. Kirtley, Rep. Prog. Phys. **73**, 126501 (2010).

[6] M. V. Moody, H. J. Paik, and E. R. Canavan, Rev. Sci. Instrum. **73**, 3957 (2002).

[7] P. Weiss, M. Knufinke, S. Bernon, D. Bothner, L. Sarkany, C. Zimmermann, R. Kleiner, D. Koelle, J. Fortagh, and H. Hattermann, Phys. Rev. Lett. **114**, 113003 (2015).

[8] J.-H. Choi, M.-S. Kim, Y.-K. Park, and M.-S. Choi, Appl. Phys. Lett. **90**, 073117 (2007).

[9] E. H. Brandt, Phys. Rev. B **55**, 14513 (1997).

[10] A. A. Babaei Brojeny and J. R. Clem, Phys. Rev. B **68**, 174514 (2003).

[11] E. H. Brandt and J. R. Clem, Phys. Rev. B **69**, 184509 (2004).

[12] J. G. E. Harris, D. D. Awschalom, F. Matsukura, H. Ohno, K. D. Maranowski, and A. C. Gossard, Appl. Phys. Lett. **75**, 1140 (1999).

[13] M. D. Chabot and J. Moreland, J. Appl. Phys. **93**, 7897 (2003).

[14] B. C. Stipe, H. J. Mamin, T. D. Stowe, T. W. Kenny, and D. Rugar, Phys. Rev. Lett. **86**, 2874 (2001).

[15] A. C. Bleszynski-Jayich, W. E. Shanks, B. Peaudecerf, E. Ginossar, F. von Oppen, L. Glazman, and J. G. E. Harris, Science **326**, 272 (2009).

[16] E. M. Q. Jariwala, P. Mohanty, M. B. Ketchen, and R. A. Webb, Phys. Rev. Lett. **86**, 1594 (2001).

[17] H. Bluhm, N. C. Koshnick, J. A. Bert, M. E. Huber, and K. A. Moler, Phys. Rev. Lett. **102**, 136802 (2009).

[18] J. Jang, R. Budakian, and Y. Maeno, Appl. Phys. Lett. **98**, 132510 (2011).

[19] H. Choi, Y. W. Kim, S.-G. Lee, J.-H. Kim, and J.-H. Choi (unpublished).

[20] D. T. Smith, J. R. Pratt, and L. P. Howard, Rev. Sci. Instrum. **80**, 035105 (2009).

[21] J. A. Sidles, J. L. Garbini, K. J. Bruland, D. Rugar, O. Zuger, S. Hoen, and C. S. Yannoni, Rev. Mod. Phys. **67**, 249 (1995).

[22] M. M. Doria, E. H. Brandt, and F. M. Peeters, Phys. Rev. B **78**, 054407 (2008).

[23] J. Kim, F. Ronning, N. Haberkorn, L. Civale, E. Nazaretski, N. Ni, R. J. Cava, J. D. Thompson, and R. Movshovich, Phys. Rev. B **85**, 180504 (2012).

[24] S. S. Rao, *Mechanical Vibrations*, 3rd ed. (Addison-Wesley, New York, 1995).

[25] G. A. Matei, E. J. Thoreson, J. R. Pratt, D. B. Newell, and N. A. Burnham, Rev. Sci. Instrum. **77**, 083703 (2006).

[26] R. J. Bruls, H. T. Hintzen, G. De With, and R. Metselaar, J. Eur. Ceram. Soc. **21**, 263 (2001).

[27] K. B. Gavan, H. J. R. Westra, E. W. J. M. van der Drift, W. J. Venstra, and H. S. J. van der Zant, Appl. Phys. Lett. **94**, 233108 (2009).